HHS Public Access

Author manuscript

Lab Chip. Author manuscript; available in PMC 2015 December 01.

Published in final edited form as:

Lab Chip. 2015 November 11; 15(23): 4441–4450. doi:10.1039/c5lc00923e.

Phenotypic drug profiling in droplet microfluidics for better targeting of drug-resistant tumors

S. Sarkar[a], **N. Cohen**[a], **P. Sabhachandani**[a], and **T. Konry**[a,†]

[a]Department of Pharmaceutical Sciences, Northeastern University, 360 Huntington Avenue, Boston, 02115 MA, USA

Abstract

Acquired drug resistance is a key factor in the failure of chemotherapy. Due to intratumoral heterogeneity, cancer cells depict variations in intracellular drug uptake and efflux at the single cell level, which may not be detectable in bulk assays. In this study we present a droplet microfluidics-based approach to assess the dynamics of drug uptake, efflux and cytotoxicity in drug-sensitive and drug-resistant breast cancer cells. An integrated droplet generation and docking microarray was utilized to encapsulate single cells as well as homotypic cell aggregates. Drug-sensitive cells showed greater death in the presence or absence of Doxorubicin (Dox) compared to the drug-resistant cells. We observed heterogeneous Dox uptake in individual drug-sensitive cells while the drug-resistant cells showed uniformly low uptake and retention. Dox-resistant cells were classified into distinct subsets based on their efflux properties. Cells that showed longer retention of extracellular reagents also demonstrated maximal death. We further observed homotypic fusion of both cell types in droplets, which resulted in increased cell survival in the presence of high doses of Dox. Our results establish the applicability of this microfluidic platform for quantitative drug screening in single cells and multicellular interactions.

Introduction

A major impediment to successful cancer treatment is the extensive heterogeneity in tumor cell populations, not only across patients but also within a tumor. Cancer cells vary widely in their response to therapy, development of drug tolerance, survival and metastatic potential. The evolution of multidrug resistant (MDR) genotype has been noted in subsets of hematologic and solid tumors including breast, ovarian, lung, and lower gastrointestinal tract cancers.[1] Clinically, patients have been known to exhibit, or increase, drug resistance even prior to the completion of therapy, suggesting rapid adaptive response in addition to inherent resistance.[2] The cellular mechanisms of drug resistance have been widely characterized in vitro by generating cell lines resistant to therapeutic agents such as anthracyclines (e.g. doxorubicin) and taxanes (e.g., paclitaxel). DNA sequencing has established that cancer cells originating from single genetic clones depict intrinsic variability in functional responses to chemotherapy.[3] Parameters such as drug inactivation, overall distribution, intracellular drug accumulation, sequestration, and efflux have been shown to be

†Corresponding author: t.konry@neu.edu.

Electronic Supplementary Information (ESI) available: [submitted]. See DOI: 10.1039/x0xx00000x

heterogeneous in many tumors.[4–6] Recently, single cell analysis revealed transcriptional heterogeneity in cell lines during the acquisition of drug tolerance, promoting the survival of a subpopulation of breast cancer cells.[7] Similar analysis performed with patient-derived xenograft tumor cells has demonstrated significant variation in intratumoral genetic signatures of single cells before and during drug treatments.[8] Thus, heterogeneity in single cell drug processing has a direct impact on cell fate and the outcome of the disease.

The conventional methods of assessing kinetic parameters associated with intracellular drug accumulation and efflux are based on flow cytometry, microscopy and plate-based assays. While flow cytometry is a powerful single cell analytical technique, it cannot be used to assess time-dependent variation in intracellular content within the same cells, or organelle-specific localization of internalized cargo in cells. Techniques such as single cell mass cytometry and capillary electrophoresis have been utilized for sensitive measurements of single cell drug uptake.[9–11] However, these methods are highly complex and yield low throughput, typically allowing the processing of 3–5 cells per hour.[12] Alternatively, automated microscopy can be used screen large numbers of cells for phenotypic indicators of dose-dependent drug activity on various targets at single cell resolution.[13]

Microfluidic devices, in combination with fluorescence microscopy, provide a high throughput platform for dynamic analysis of cellular function with single cell resolution. Microfluidic single cell analysis has many advantages including high sensitivity, accuracy, multiplexing, and precise control of cellular microenvironment.[14,15] Several microfluidic approaches have been developed for drug cytotoxicity analysis and chemical library screening.[16–24] In a proof of concept study, chemical gradient generators were integrated with microcavities to investigate cytotoxicity of potassium cyanide on single HeLa cells.[21] Centrifugal microfluidics-based cell traps were used to isolate single cardiomyocytes and evaluate the effect of drugs on long term growth and cellular dynamics.[24] Drug uptake and efflux in the same cell was characterized by serial treatment of wild type as well as vinblastine-resistant leukemia cells with daunorubicin and control media.[25] The authors further evaluated the effect of P-gp inhibitor verapamil on drug retention in cells. This method was extremely low throughput, allowing a single cell to be characterized at one time. Furthermore, the study did not correlate the cytotoxic effect of the drugs or MDR modulators on single cells. Doxorubicin (Dox) uptake and P-gp expression was assessed in single cells following cell lysis and laser-induced fluorescence detection.[23] An average throughput of 6–8 cells per min was reported; however, the necessity of cell lysis negated dynamic analysis of drug uptake over longer time periods.

High throughput droplet microfluidics strategies have been used to assess genetic and proteomic content of single cells, so as to provide insights regarding cell responses to extrinsic stimuli and cell fate in normal or diseased states.[26,27] Microfluidic droplets were applied for cytotoxic screening of mammalian and yeast cells.[28–31] A chemical library of various mitomycin C concentrations were encapsulated in droplets with single cells over a period of four days.[28] A combinatorial screening of anti-cancer drugs and cell cycle inhibitors was used to treat lung cancer cells in droplets, although not in single cells.[30] Complex droplet manipulations were performed to deliver drugs in specific combinations and schedules to obtain maximal apoptosis induction. A significant advantage of droplet

microfluidics-based approaches is the ability to compartmentalize single cells, thus eliminating cross-communication with neighboring cells. Signaling through paracrine mechanisms between homotypic and heterotypic cells results in increasing cancer survival and therapeutic resistance.[32,33] Furthermore, apoptosis-related cellular processes can initiate or deactivate responses in surrounding cells.[34,35] Droplet microfluidics provides a suitable platform for characterizing cytotoxic drug uptake and apoptosis in single cells without affecting the functionality of adjacent cells.

In this study we utilized an integrated microfluidic droplet array platform to analyse Dox uptake in wild type and Dox-resistant breast cancer cells. We observed variable Dox uptake and retention characteristics in single wild type (Dox-sensitive) cells whereas Dox-resistant cells showed near-uniform low levels of Dox accumulation. We determined that a relatively small population of drug-resistant cells retained the ability to incorporate extracellular materials for longer durations, although they demonstrated rapid extrusion profiles compared to the wild type cells. These cells also showed increased cell death compared to the rest of the population, suggesting that transient increase in intracellular Dox could be sufficient to activate death-related signalling pathways. In droplets encapsulating more than one homotypic cell, we observed cytoplasmic fusion between the cells, associated with distinct survival advantage over single cells in the presence of high Dox concentrations. Drug-resistant cell phenotypes further showed aberrant nuclear division and cytoplasmic protrusions in droplets. Our findings suggest that this droplet microfluidic array is a promising tool for assessing dynamic parameters related to multidrug resistance in single cells in a high-throughput manner.

Experimental

Microfluidic droplet array fabrication

The microfluidic droplet generator and docking array platform was designed using CAD (CAD/ Art Services, Bandon, OR) and printed on a transparency photomask (Fine Line Imaging, Colorado Springs, CO). The masks were used to develop silicon wafer templates by spin-coating negative photo resist SU-8 2100 (MicroChem, Newton, MA) to a thickness of 150 μm followed by UV photolithography. Poly(dimethylsiloxane) (PDMS) (Sylgard 184, Dow Corning, Midland, MI) devices were prepared from the master templates via standard soft lithography procedure. PDMS was mixed at a 10:1 ratio (w/w) with the silicone elastomer curing agent, poured over the wafer, degassed and cured for 12 h at 65 °C. Each device was bonded to a glass slide that was treated with plasma oxidation, followed by heat treatment at 90 °C for 10 min.

The devices consisted of three inlets and two outlets. The aqueous suspensions containing cells and drugs were incubated separately through two of the inlets, while fluorinated oil (Fluorinert® FC-40, Sigma, St. Louis, MO) was added through a specifically designed inlet. The droplets were formed due to shearing of the aqueous phase by the oil at a T-shaped nozzle and stabilized by the addition of 2% w/w surfactant (008-FluoroSurfactant, Ran Biotechnologies, Beverly, MA). The droplets were docked in a 1000 site-microarray for functional assessment. Prior to the addition of aqueous phase, the devices were made hydrophobic by treating with Aquapel (Aquapel, Pittsburg, USA) for 15 min followed by air

flushing. All fluid phases were introduced into the device from syringes connected through Tygon Micro Bore PVC Tubing of the following dimension: 0.010″ ID, 0.030″ OD, 0.010″ wall (Small Parts Inc., FL, USA). Syringe pumps (Harvard Apparatus, USA) were used to control flow rates from each inlet. The ratio of the oil to aqueous flow rates were maintained at a ratio of 4:1 to obtain optimal droplet sizes. The microfluidic array containing cells was maintained in a humidified microscopic stage-top incubator at 37 °C and 5% CO_2 for the duration of the experiment.

MCF-7 cell culture and ABCB1 mRNA detection

Wild type MCF-7 human breast adenocarcinoma cells were originally purchased from American Type Culture Collection (ATCC, Manassas, VA) and generously provided by Dr. Vladimir Torchilin, Northeastern University, Boston, MA. Cells were routinely passaged every three days and seeded at a density of 1×10^6 cells/mL.

Detection of ABCB1 mRNA in droplet-encapsulated live MCF-7 cells was performed using SmartFlare nanoprobes (EMD Millipore, Billerica, MA). Cy5-conjugated ABCB1 mRNA (#SF-2394) stock solution was diluted as per the manufacturer's instructions. The final ratio of cells to the diluted probe was maintained at 1×10^6 cells: 100 μL. The probes and cells were incubated through separate inlets and maintained in the dark for 24 h. For probe uptake in adherent cells, 20,000 cells drug-sensitive or -resistant MCF-7 cells were seeded in a 96-well plate and allowed to adhere overnight. 4 μL of the diluted probe was added to the wells and observed for the next 24 h. The cells were periodically imaged using a Cy5 filter.

Development of Dox-resistant cell line

Dox-resistant MCF-7 cells were generated as per established protocols following single step selection.[36] Briefly, 2×10^6 cells were seeded in a culture flask and 20 μM of Dox solution was added to the cells for 48 h. The cells were rinsed with fresh media and allowed to grow for another 48 h. Cells still alive after Dox removal were harvested and expanded in culture over the next week. The subclones that demonstrated maximal (98–100%) viability were selected for experiments. The dose –dependent viability of this line was determined in microplate analysis (Supplementary Fig. S1). The parental and derived cell lines were maintained in DMEM medium with 4.5 g/L glucose and L-glutamine (Corning Cellgro, Manassas, VA) supplemented with 10% Fetal Bovine Serum (Corning) and 1% antibiotic-antimycotic (Corning). All cells were cultured at 37 °C under 5% CO_2 in a humidified atmosphere.

Dox uptake and cytotoxicity analysis

Doxorubicin hydrochloride (Dox) was purchased from LC Laboratories (Woburn, MA). Stock solutions of Dox were prepared at a concentration of 7 mM in sterile water and stored at 4 °C. Dox was diluted to 12.8 μM in complete growth media immediately prior to use. MCF-7 (wild type or Dox-resistant) cells were incubated through one inlet of the microfluidic device at a concentration of 1×106 cells/mL while Dox was incubated through a separate inlet to ensure that drug exposure occurred only in droplets. The droplets containing single cells were identified and imaged via time-lapse microscopy over 24 h. Dox

uptake was assessed using a DsRed filter (Peak Ex/Em-577/602nm) as the excitation and emission wavelengths of Dox are 470 and 585 nm respectively.

Based on dose-dependent responses in microplates, 3.2 μM and 12.8 μM Dox were used for cytotoxicity analysis (Fig. S1). MCF-7 Dox-resistant cells were treated to an additional concentration of 30 μM of Dox. Control cells were incubated in droplets with only growth media (i.e., no Dox). Assessment of cell viability was carried out using a combination of chemical and morphological indicators (Supplementary Fig. S2).

Cell viability and efflux studies

Previous research has established that 90% adherent cells survive in droplets for at least 2 days.[69] Addition of viability probes to microfluidic cancer cell cultures does not significantly impact cell viability or proliferation over a period of 72 h.[20] Therefore, cell viability analysis was performed by incorporating Live/Dead Viability/Cytotoxicity Assay reagents: calcein AM and ethidium homodimer-1 (EthD-1) (Life Technologies, Carlsbad, CA). The final concentration of calcein AM and EthD-1 was maintained at 2 μM and 4 μM respectively. The reagents and the cells were incubated through separate channels for viability analysis in droplets. Calcein AM, the live cell indicator, was assessed by time-lapse microscopy at excitation/emission: 494/517 nm. EthD-1, the dead cell indicator, was read at 528/617 nm. The proportion of live cells was calculated as a ratio of the number of live cells to the total number of cells as expressed as ‘percentage viability’. All cells were labeled with Hoechst nuclear dye as per the manufacturer’s recommendation.

Since the emission spectra of Dox overlaps with EtHd-1, we performed a direct comparison of Dox fluorescence and EtHd-1 fluorescence in fixed cells. EtHd-1 fluorescent intensity in the nucleus was ≥ 10-fold higher than Dox fluorescence in all monitored cells. Therefore, a definitive indication of cell death based on EtHd-1 incorporation was made only where nuclear fluorescence exceeded a pre-set threshold. Additionally, we considered the following morphological markers while assessing cell viability of Dox-treated cells: significant cell blebbing followed by membrane rupture, cytoplasmic fragmentation, nuclear shrinkage and condensation indicated by increased Hoechst intensity (Supplementary Fig. S2).

Cell efflux in droplets was characterized by labeling 1×10^6 MCF-7 cells off-chip with 2 μM Calcein AM for 30 min at 37 °C, followed by repeated washing of cells to remove excess labelling solution. The cells were incubated in droplets with or without Dox. The droplets were imaged serially over 24 h by automated time-lapse microscopy.

Calculation of single cell efflux times

The fluorescence intensity (I) of Calcein was measured as a function of time with ImageJ software as detailed below. To quantify the rate of calcein loss due to efflux, time-varying decay profiles obtained from single cells were fitted to a sum of two exponentials:

$$I=I_0+Ae\left(\frac{-t}{\tau_1}\right)+Be\left(\frac{-t}{\tau_2}\right)$$

The average lifetime (τ) of Calcein in a cell was calculated as

$$\tau = \tau_1 \tau_2 / \tau_1 + \tau_2.$$

The parameters I_0, coefficients A and B and the lifetimes τ_1 and τ_2 were obtained via MATLAB-based curve fitting. The mean decay time ± standard deviation of the two cell population is represented here.

Image acquisition, processing and statistical analysis

The phase/fluorescent images of cells in droplets were captured using Zeiss Axio Observer.Z1 Microscope (Zeiss, Germany) equipped with a Hamamatsu digital camera C10600 Orca-R2, 10–40x objectives and standard FITC/DAPI/DsRed filters. Time-lapse images were obtained every hour by automated software control, using Zen imaging program (Zeiss), for a total period of 24 h. Comparative studies of Dox uptake and Calcein AM efflux profiling of Dox-sensitive and –resistant cells was done by utilizing identical microscope settings. Post-data acquisition image processing and analysis was done with ImageJ (http://rsb.info.nih.gov/ij/), Microsoft Office Excel 2010, and Origin Pro software. Fluorescent intensity of the cells at every time point was analyzed by selecting the region of interest (i.e., the cell body) and measuring mean intensity in ImageJ. After background correction, normalized fluorescent intensity (NFI) of each cell was calculated as a ratio of fluorescent intensity at every time point with respect to fluorescent intensity at the initial time. All statistical analysis was performed using Student's t test, and p value <0.05 was considered statistically significant.

Results and Discussion

Single cell encapsulation in droplet array

We encapsulated single MCF-7 breast cancer cells and Dox in picoliter volume droplets in an integrated microfluidic droplet array. Monodisperse droplets were generated at optimized flow rates by incubating the cell suspension through one inlet and Dox-containing media through the other inlet (Fig. 1). The device design incorporates a 2.05 cm-long serpentine segment prior to the droplet generation junction to promote lateral ordering of cells.[37] The droplet sizes were maintained at ~100 μm diameter (i.e., 520 pL volume). Although small droplet sizes permit efficient mixing of encapsulated reagents, we observed that further reduction in droplet diameter compromised cell viability in multiple cell lines over long experimental duration. The droplets were subsequently directed to a parallelized docking array consisting of sequential trapping sites spaced optimally to prevent contact-mediated coalescence over longer durations. The trapping sites were numbered so as to facilitate dynamic monitoring of the same droplets, thus permitting analysis of the same single cells instead of distinct single cells in a population. Previous on-chip incubation strategies included adding delay lines that allowed longer droplet storage without altering back pressure.[28] However, droplets were collected off-chip for prolonged cell incubation, which necessitated the development of optical barcoding approaches to track individual droplets throughout the processing stages. In our study, this issue was resolved by retaining the

droplets on-chip in specific locations in the integrated docking array. Once trapped, the droplets were held stably in the array for over 24 h in a humidified environment that minimized droplet shrinking. This approach allowed us to assess 10^3 droplets simultaneously.[38]

Since cell encapsulation in droplets is governed by Poisson probability, we observed blank, single cell-loaded and multicellular droplets in the array. In all experiments, viability/cytotoxicity studies were restricted to droplets that contained individual cells (Figs. 1, 2). Cell fusion studies, in the presence or absence of Dox, were conducted in droplets containing 2–4 cells (Fig. 5). Our approach established the feasibility of comparing single cell phenotypic response as well as homotypic interactions between encapsulated cells from the same population.

On-chip cytotoxicity analysis of Dox-sensitive vs. Dox-resistant MCF-7 cells

We characterized cytotoxicity of Dox on both Dox-sensitive and Dox-resistant MCF-7 cells at single cell resolution in droplets (referred to as MCF-7S and MCF-7R respectively). MCF-7S cells showed greater viability in the absence of Dox compared to two doses of Dox treatment, as also observed in bulk cell experiments (64% vs. 16–30%). However, we did not detect a significant difference in Dox-induced cell death between 3.2 μM and 12.8 μM Dox in single cells in the 24 h period (Fig. 2A). Bulk cell viability assays in adherent MCF-7 cultures showed significant difference Dox-induced cell death at these doses only after 48 h (Supplementary Fig. S1). Although the MCF-7 cells are normally assessed under anchorage-dependent culture conditions, they have been tested previously in suspension cultures and found to be functional).[39,40] We further tested uptake capabilities of these cells in droplets with ABCB1 mRNA probes (Fig. 1 and Supplementary Fig. S1). Single MCF-7S cells showed endocytosis of the nanoprobes and fluorescent detection of ABCB1, the gene that encodes for P-gp within the same time frame as adherent cells. Our results suggest that the cells retain functionality in aqueous droplets, at least up to 24 h. Therefore, the microfluidic droplet platform can be utilized to perform cytotoxic screening of adherent cells, with the added advantage of single cell analysis and dynamic spatiotemporal resolution.

We generated Dox-resistant MCF-7 cells as described in the Experimental section. Morphologically, the MCF-7R cells showed distinctive features compared to the MCF-7S cells, including multiple vesicles (Fig. S1) and multi-nucleation (Fig. 5).[41] We observed accumulation of extracellular materials (e.g., Calcein AM) in these vesicles under suspension conditions. In contrast with the MCF-7S cells, viability of untreated single MCF-7R cells was higher (76% vs 64% at 18 h) in the droplets (Fig 2B). Treatment of the drug-resistant cells with 12.8μM Dox depicted no significant change in viability compared to untreated cells, resulting in ≥4-fold increase in viability compared to the drug-sensitive cell line. However, treatment of MCF-7R cells with 30μM Dox, resulted in significant cell death. The MCF-7S cells depicted membrane blebbing and rupture following sustained Dox treatment in the droplets (Fig. 2C), while MCF-7R cells depicted pronounced morphological deformation, similar to the hallmarks of apoptosis, in the droplets (Fig. 2D).[42] MCF-7R cell death was associated with condensed nuclear matter, cell shrinkage, extensive blebbing and cytoplasmic fragmentation (Fig. 2D and Supplementary Fig. S2).

Dox is a commonly used anticancer drug for treatment of various malignancies, including breast and liver cancer.[43] Dox intercalation with DNA causes DNA damage, free radical generation, activation of NF-κB, p53 and caspases and subsequently leads to apoptotic cell death.[44–46] Dox-induced cell death is dependent on differential molecular mechanisms in normal cells and cancer cells, [47] as well as on the doses and scheduling of drugs delivered.[48] Resistance to Dox has been observed in breast cancer patients undergoing chemotherapy due to acquired mutations in the P53 gene.[49] Dox resistance has also been related to the overexpression of ATP-dependent efflux pumps, the ATP-binding cassette (ABC) transporters possessing broad drug specificity. The transmembrane P-glycoprotein (P-gp) encoded by the ABCB1 gene is the most studied transporter due to its upregulation in response to multiple drugs in cancer. [50,51] We verified that the wild type MCF-7S cells expressed ABCB1; however, ABCB1 mRNA was not detected in live cells in the MCF-7R cells in droplets (data not shown). The Dox-resistant MCF-7 phenotype has been previously characterized as overexpressing the MDR-1 (ABCB1) gene.[41] We hypothesize that the nanoprobes were eliminated from the cells prior to fluorescent activation due to increased efflux. Additionally, recent evidence suggests that these drug-resistant cell lines possess reduced ability to ingest extracellular materials due to diminished capacity for endocytosis, which could have contributed to the lack of detection.[52]

Dynamic assessment of Dox uptake by MCF-7 cells

The efficacy of Dox in cancer cell killing is dependent on a number of factors including drug uptake, intracellular drug retention, localization in cytoplasm and cellular organelles and efflux. We assessed variability in Dox uptake by single drug-sensitive and –resistant cells in the microfluidic droplet array. Incubation of the Dox and MCF-7S/MCF-7R cells through separate channels ensured that the cells were exposed to Dox only within the droplets. Previous studies have shown that Dox exhibits autofluorescence, which can be detected primarily in the nuclei of drug-sensitive breast cancer cells.[41] We developed dynamic profiles of Dox uptake over a period of 21 h by serial fluorescent imaging of single cells. MCF-7S cells demonstrated strong heterogeneity in Dox uptake and retention over time; 67% of the cells showed relatively small (<0.5 fold change over 6 h) changes in intracellular Dox levels, 32% of cells showed increase in Dox uptake and 1% cells showed loss of Dox (Fig. 3A,B). In agreement with previous reports, we found more accumulation of Dox in the nuclei of MCF-7S cells compared to the cytoplasm.

In contrast, MCF-7R cells showed minimal accumulation of Dox that remained consistent over 6 h period (Fig. 3C). Drug-resistant breast cancer cells are known to sequester Dox in intracellular compartments, such as vesicles,[41,67] and prevent Dox interaction with DNA, to minimize Dox-induced DNA damage. We did not observe this in the droplet-encapsulated MCF-7R cells. Instead, we found diffuse accumulation in the cytoplasm and nucleus of the cells that showed low levels of Dox uptake. Difference in Dox uptake has been noted previously in adherent monolayer studies, where the resistant cells not only depicted two-fold less Dox uptake but also a slower rate of uptake compared to wild type cells.[53] Pre-treatment of the Dox-resistant cells with P-gp inhibitors resulted in increasing drug accumulation in bulk cultures of resistant cells as well as in single cells.[25,53] While the single cell analysis study was primarily focused on rapid uptake quantification by transiently

(in the order of min) exposing cells to drugs, we characterized drug uptake of the same cells over longer periods by sustained drug exposure. In pathological situations, chemotherapy drugs are expected to remain in circulation for hours before renal clearance. This affects not only the localized, highly adhesive primary tumor cells but also circulating tumor cells. Although our platform was used to model single cell Dox uptake events in this study, we envision future studies to assess the effect of combinatorial drug screening of various types of cells with differential surface properties.

Comparative profile of Calcein AM efflux by MCF-7 cells

We subsequently assessed the ability of MCF-7 cells to efflux intracellular cargo. Rapid efflux was detected in single cells in the absence of drugs,[25,54] and could be a contributing factor in the reduced intracellular Dox in MCF-7R cells in the droplets. We utilized Calcein AM, a live cell indicator that exhibits high levels of fluorescence in cells, to identify subpopulations that display varied phenotypes with respect to both uptake and efflux. Non-fluorescent Calcein AM freely diffuses into cells and is trapped by the cleavage of acetoxymethyl groups by esterases. MDR transporter proteins mediate extrusion of Calcein AM and Calcein from the cells, resulting in loss of intracellular fluorescence. Therefore, Calcein efflux assay is considered a functional indicator of MDR activity.[55–57] We observed that the encapsulated MCF-7R cells could be divided into three distinct subtypes based on high, medium and minimal levels of Calcein AM fluorescence (Fig. 4A). More than 50% of the cells monitored showed very low or no Calcein fluorescence despite repeated labelling efforts with varying doses and incubation times of the dye. This finding contrasted with the MCF-7S cells, which overwhelmingly depicted high or medium levels of Calcein fluorescence (71% and 20% respectively). MCF-7R cells that did show Calcein uptake also demonstrated significantly faster efflux times (3.07 h ± 1.87) compared to the MCF-7S cells (5.43 h ± 3.53), suggesting that Dox-resistant cells had upregulated transporter proteins (Fig. 4C, D).

We then determined the fate of the MCF-7R cell subsets in response to Dox treatment. We found that greatest proportion of cell death (58%) occurred in the subset of cells that exhibited high Calcein AM fluorescence initially (Fig. 4B), while the cells that showed least Calcein fluorescence also depicted the least death (27%). This result not only establishes the heterogeneity in MCF-7R cells in vitro but also correlates single cell viability to the functional activity of efflux transporter proteins. Based on our findings, we conclude that the MCF-7R cells with high to medium Calcein fluorescence represent phenotypes capable of drug retention, however transiently, due to lower activity of the MDR transporter. This leads to increased cell death. MCF-7R cells that show minimal or no Calcein fluorescence either possess nominal uptake ability or highly active transporters that minimize intracellular Dox levels. Consequently, these cells present decreased drug-induced cytotoxic stress and death.

Homotypic cell fusion and incomplete division in droplets

We consistently observed homotypic cell fusion in droplets that contained more than one cell (Fig. 5A). Cell fusion was primarily restricted to cytoplasmic merging, resulting in cells with multiple nuclei. Cell fusion was not related to drug resistivity as both MCF-7 lines depicted aggregation and merging in droplets. Likewise, Dox did not have any effect on the

extent of cell fusion since the proportion of merging events was similar in the presence and absence of Dox (8.97% vs. 13.74% respectively for MCF-7R cells). Cell death in the fusogenic subset was generally lower than in the overall population (Fig. 5B), although there was broad variability in the number of cells involved and the timing of fusion events in the droplets.

Cancer cells undergo homotypic and heterotypic cell fusion in vitro.[58] Cell fusion is thought to play vital roles in various aspects of tumor progression, including aneuploidy and tumorigenesis, drug resistance, development of cancer stem cells and metastasis. The fusion of two cancer cells resistant to different drugs resulted in a hybrid line that was resistant to multiple drugs.[59] Dox is known to induce homotypic and heterotypic fusion in transfected MCF-7 cells.[60] However, no fusion events were observed in the absence of Dox or in drug-resistant cells. Our findings show a more comprehensive fusion program occurring in MCF-7 cells in suspension. It is feasible that the cells aggregate in suspension to promote survival, as observed in circulating tumor cells mediated by proteins such as galectin-3 and MUC1.[61,62] Side populations of MCF-7 cells express MUC1, and both drug-sensitive and –resistant variants of MCF-7 cells express galectin-3.[40,63] We hypothesize that interactions between these proteins could have led to the initial homotypic aggregation in droplets, which facilitated cell fusion.

We further observed ≤1% of cells undergoing aberrant morphological phenomena where the nucleus divided into multiple nuclei followed by complete or incomplete cytoplasmic separation. As shown in Fig. 5C, the nuclear region divided into three segments while the cytoplasm appeared to divide into two compartments that did not fully separate over the time course. This event ended with widespread cytoplasmic blebbing and potential cell death. The presence of cytotoxic drugs can promote mitotic catastrophe in cells, which is described as aberrant mitosis due to atypical chromosome segregation, leading to necrotic or apoptotic cell death.[64–66] While the precise nature of cell death program mediated in droplets is beyond the scope of this study, we note that the integrated droplet microarray allows simultaneous investigation of single cell-specific events as well as homotypic cell interactions without requiring further optimization of the experimental platform.

Conclusions

In conclusion, the integrated droplet microfluidic platform allowed functional characterization of drug-related cytotoxicity in single and multiple cells in the same experiment. We utilized this technique to assess phenotypic heterogeneity in uptake, efflux and subsequent cell death in drug sensitive and resistant variants of a tumor cell line. This approach can be further extended to determine the molecular mechanisms of multidrug resistance in single cells by systematic screening of a library of anticancer therapeutics. Dox resistance has been linked to modification of intracellular protein cascades such as MAPK and cyclins.[68] Improved adaptation to stress, DNA damage repair, apoptotic deficiency, and epigenetic modifications are also important contributing factors in the failure of targeted chemotherapy and require analysis at single cell resolution. Additionally, the platform can be applied for evaluation of homotypic and heterotypic cellular interactions, which play critical roles in regulating the response of cancer cells to extracellular stimuli. Events such

as cell fusion and mitotic failure contribute to genomic instability in tumors. The droplet microarray device described here can be used to profile pharmacological effect of drugs in various disease contexts and as clinical prognostic assays for personalized medicine.

Supplementary Material

Refer to Web version on PubMed Central for supplementary material.

Acknowledgments

The authors acknowledge their funding source NIH/NCI for supporting this study. The authors are grateful to Sai Srinivas Mynampati at Northeastern University for assistance in routine fabrication of microfluidic devices.

References

1. Gottesman MM. Annu Rev Med. 2002; 53:615–627. [PubMed: 11818492]
2. Goldman A, Majumder B, Dhawan A, Ravi S, Goldman D, Kohandel M, Majumder PK, Sengupta S. Nat Commun. 2015; 6:6139. [PubMed: 25669750]
3. Kreso A, O'Brien CA, Van Galen P, Gan OI, Notta F, Brown AM, Ng K, Ma J, Wienholds E, Dunant C, Pollett A, Gallinger S, McPherson J, Mullighan CG, Shibata D, Dick JE. Science. 2013; 339:543–438. [PubMed: 23239622]
4. Minchinton AI, Tannoc IF. Nat Rev Cancer. 2006; 6:583–592. [PubMed: 16862189]
5. Krishan A. Cytometry. 1995; 21:72–75. [PubMed: 8529475]
6. Lockman PR, Mittapalli RK, Taskar KS, Rudraraju V, Gril B, Bohn KA, Adkins CE, Roberts A, Thorsheim HR, Gaasch JA, Huang S, Palmieri D, Steeg PS, Smith QR. Clin Cancer Res. 2010; 16:5664–5678. [PubMed: 20829328]
7. Lee MC, Lopez-Diaz FJ, Khan SY, Tariq MA, Dayn Y, Vaske CJ, Radenbaugh AJ, Kim HJ, Emerson BM, Pourmand N. Proc Natl Acad Sci USA. 2014; 111:E4726–35. [PubMed: 25339441]
8. Kim KT, Lee HW, Lee HO, Kim SC, Seo YJ, Chung W, Eum HH, Nam DH, Kim J, Joo KM, Park WY. Genome Biol. 2015; 16:127. [PubMed: 26084335]
9. Bendall SC, Simonds EF, Qiu P, Amir el-AD, Krutzik PO, Finck R, Bruggner RV, Melamed R, Trejo A, Ornatsky OI, Balderas RS, Plevritis SK, Sachs K, Pe'er D, Tanner SD, Nolan GP. Science. 2011; 332:687–696. [PubMed: 21551058]
10. Meredith GD, Sims CE, Soughayer JS, Allbritton NL. Nat Biotechnol. 2000; 18:309–312. [PubMed: 10700147]
11. Malek AH, Khaledi MG. Electrophoresis. 2003; 24:1054–1062. [PubMed: 12658695]
12. Borland LM, Kottegoda S, Phillips KS, Allbritton NL. Annu Rev Anal Chem (Palo Alto Calif). 2008; 1:191–227. [PubMed: 20636079]
13. Perlman ZE, Slack MD, Feng Y, Mitchison TJ, Wu LF, Altschuler SJ. Science. 2004; 306:1194. [PubMed: 15539606]
14. Mark D, Haeberle S, Roth G, von Stetten F, Zengerle R. Chem Soc Rev. 2010; 39:1153–1182. [PubMed: 20179830]
15. Guo F, French JB, Li P, Zhao H, Chan CY, Fick JR, Benkovic SJ, Huang TJ. Lab Chip. 2013; 13:3152–3162. [PubMed: 23843092]
16. Wang Z, Kim MC, Marquez M, Thorsen T. Lab Chip. 2007; 7:740–745. [PubMed: 17538716]
17. Wada K, Taniguchi A, Kobayashi J, Yamato M, Okano T. Biotechnol Bioeng. 2008; 99:1513–1517. [PubMed: 18080341]
18. Li X, Ling V, Li PCH. Anal Chem. 2008; 80:4095–4102. [PubMed: 18447319]
19. Zhao L, Cheng P, Li J, Zhang Y, Gu M, Liu J, Zhang J, Zhu JJ. Anal Chem. 2009; 81:7075–7080. [PubMed: 19634888]
20. Wlodkowic D, Skommer J, McGuinness D, Faley S, Kolch W, Darzynkiewicz Z, Cooper JM. Anal Chem. 2009; 81:6952–6959. [PubMed: 19572560]

21. Hosokawa M, Hayashi T, Mori T, Yoshino T, Nakasono S, Matsunaga T. Anal Chem. 2011; 83:3648–3654. [PubMed: 21526753]
22. Miller OJ, El Harrak A, Mangeat T, Baret JC, Frenz L, El Debs B, Mayot E, Samuels ML, Rooney EK, Dieu P, Galvan M, Link DR, Griffiths AD. Proc Natl Acad Sci U S A. 2012; 109:378–383. [PubMed: 22203966]
23. Deng B, Tian Y, Yu X, Song J, Guo F, Xiao Y, Zhang Z. Anal Chim Acta. 2014; 820:104–111. [PubMed: 24745743]
24. Espulgar W, Aoki W, Ikeuchi T, Mita D, Saito M, Lee J-K, Tamiyaa E. Lab Chip. 201510.1039/C5LC00652J
25. Li X, Chen Y, Li PCH. Lab Chip. 2011; 11:1378–1384. [PubMed: 21327253]
26. Anand RK, Chiu DT. Curr Opin Chem Biol. 2012; 16:391–399. [PubMed: 22694875]
27. Guo MT, Rotem A, Heyman JA, Weitz DA. Lab Chip. 2012; 12:2146–2155. [PubMed: 22318506]
28. Brouzes EE, Medkova M, Savenelli N, Marran D, Twardowski M, Hutchison JB, Rothberg JM, Link DR, Perrimon N, Samuels ML. Proc Natl Acad Sci USA. 2009; 106:14195–14200. [PubMed: 19617544]
29. Churski K, Kaminski TS, Jakiela S, Kamysz W, Baranska-Rybak W, Weibel DB, Garstecki P. Lab Chip. 2012; 12:1629–1637. [PubMed: 22422170]
30. Du GS, Pan JZ, Zhao SP, Zhu Y, den Toonder JM, Fang Q. Anal Chem. 2013; 85:6740–6747. [PubMed: 23786644]
31. Kumar PT, Vriens K, Cornaglia M, Gijs M, Kokalj T, Thevissen K, Geeraerd A, Cammue BPA, Puersf R, Lammertyn J. Lab Chip. 2015; 15:1852–1860. [PubMed: 25710603]
32. Boelens MC, Wu TJ, Nabet BY, Xu B, Qiu Y, Yoon T, Azzam DJ, Twyman-Saint Victor C, Wiemann BZ, Ishwaran H, ter Brugge PJ, Jonkers J, Slingerland J, Minn AJ. Cell. 2014; 159:499–513. [PubMed: 25417103]
33. Damhofer H, Veenstra VL, Tol JA, van Laarhoven HW, Medema JP, Bijlsma MF. J Cell Sci. 2015; 128:129–139. [PubMed: 25359882]
34. Bournazou, Pound JD, Duffin R, Bournazos S, Melville LA, Brown SB, Rossi AG, Gregory CD. J Clin Invest. 2009; 119:20–32. [PubMed: 19033648]
35. Gregory CD, Pound JD, Devitt A, Wilson-Jones M, Ray P, Murray RJ. MAbs. 2009; 1:370–376. [PubMed: 20068393]
36. Calcagno AM, Fostel JM, To KKW, Salcido CD, Martin SE, Chewning KJ, Wu CP, Varticovski L, Bates SE, Caplen NJ, Ambudkar SV. Br J Cancer. 2008; 98:1515–1524. [PubMed: 18382425]
37. Edd JF, Di Carlo D, Humphry KJ, Köster S, Irimia D, Weitz DA, Toner M. Lab Chip. 2008; 8:1262–1264. [PubMed: 18651066]
38. Golberg A, Linshiz G, Kravets I, Stawski N, Hillson NJ, Yarmush ML, Marks RS, Konry T. PLoS One. 2014; 9:e86341. [PubMed: 24475107]
39. Pourreau-Schneider N, Berthois Y, Mittre H, Charpin C, Jacquemier J, Martin PM. J Steroid Biochem. 1984; 21:763–771. [PubMed: 6527540]
40. Engelmann K, Shen H, Finn OJ. Cancer Res. 2008; 68:2419–2426. [PubMed: 18381450]
41. AbuHammad S, Zihlif M. Genomics. 2013; 101:213–220. [PubMed: 23201559]
42. Saraste A, Pulkki K. Cardiovasc Res. 2000; 45:528–537. [PubMed: 10728374]
43. Minotti G, Menna P, Salvatorelli E, Cairo G, Gianni L. Pharmacol Rev. 2004; 56:185–229. [PubMed: 15169927]
44. Gewirtz DA. Biochem Pharmacol. 1999; 57:727–741. [PubMed: 10075079]
45. Koceva-Chyla A, Jedrzejczak M, Skierski J, Kania K, Jozwiak Z. Apoptosis. 2005; 10:1497–1514. [PubMed: 16215684]
46. Suzuki F, Hashimoto K, Kikuchi H, Nishikawa H, Matsumoto H, Shimada J, Kawase M, Sunaga K, Tsuda T, Satoh K, Sakagami H. Anticancer Res. 2005; 25:887–893. [PubMed: 15868924]
47. Wang S, Konorev EA, Kotamraju S, Joseph J, Kalivendi S, Kalyanaraman B. J Biol Chem. 2004; 279:25535–25543. [PubMed: 15054096]
48. Riganti C, Gazzano E, Gulino GR, Volante M, Ghigo D, Kopecka J. Cancer Lett. 2015; 360:219–226. [PubMed: 25681670]

49. Aas T, Børresen AL, Geisler S, Smith-Sørensen B, Johnsen H, Varhaug JE, Akslen LA, Lønning PE. Nat Med. 1996; 2:811–814. [PubMed: 8673929]
50. Savas B, Cole SP, Akoglu TF, Pross HF. Nat Immun. 1992; 11:177–192. [PubMed: 1358293]
51. Lockhart AC, Tirona RG, Kim RB. Mol Cancer Ther. 2003; 2:685–698. [PubMed: 12883042]
52. Pisco AO, Jackson DA, Huang S. Front Oncol. 2014; 4:306. [PubMed: 25401091]
53. Shen F, Chu S, Bence AK, Bailey B, Xue X, Erickson PA, Montrose MH, Beck WT, Erickson LC. J Pharmacol Exp Ther. 2008; 324:95–102. [PubMed: 17947497]
54. Willingham MC, Cornwell MM, Cardarelli CO, Gottesman MM, Pastan I. Cancer Res. 1986; 46:5941–5946. [PubMed: 3756931]
55. Homolya L, Holló M, Müller M, Mechetner EB, Sarkadi B. Br J Cancer. 1996; 73:849–855. [PubMed: 8611394]
56. Legrand O, Simonin G, Perrot JY, Zittoun R, Marie JP. Blood. 1998; 91:4480. [PubMed: 9616142]
57. Ansbro MR, Shukla S, Ambudkar SV, Yuspa SH, Li L. PLoS One. 2013; 8:e60334. [PubMed: 23593196]
58. Lu X, Kang Y. Cancer Res. 2009; 69:8536–8539. [PubMed: 19887616]
59. Miller FR, McInerney D, Rogers C, Miller BE. J Cell Biochem. 1988; 36:129–136. [PubMed: 3356752]
60. Yang JY, Ha SA, Yang YS, Kim JW. BMC Cancer. 2010; 10:388. [PubMed: 20649952]
61. Glinsky VV, Glinsky GV, Glinskii OV, Huxley VH, Turk JR, Mossine VV, Deutscher SL, Pienta KJ, Quinn TP. Cancer Res. 2003; 63:3805–3811. [PubMed: 12839977]
62. Zhao Q, Barclay M, Hilkens J, Guo X, Barrow H, Rhodes JM, Yu LG. Mol Cancer. 2010; 9:154. [PubMed: 20565834]
63. Satelli A, Rao PS, Gupta PK, Lockman PR, Srivenugopal KS, Rao US. Oncol Rep. 2008; 19:587–594. [PubMed: 18288388]
64. Castedo M, Perfettini JL, Roumier T, Andreau K, Medema R, Kroemer G. Oncogene. 2004; 23:2825–2837. [PubMed: 15077146]
65. Eom YW, Kim MA, Park SS, Goo MJ, Kwon HJ, Sohn S, Kim WH, Yoon G, Choi KS. Oncogene. 2005; 24:4765–4777. [PubMed: 15870702]
66. Grzanka D, Grzanka A, Izdebska M, Gackowska L, Stepien A, Marszalek A. Oncol Rep. 2010; 23:655–663. [PubMed: 20127003]
67. Venne A, Li S, Mandeville R, Kabanov AA, Alakhov V. Cancer Res. 1996; 56:3626. [PubMed: 8705995]
68. Smith L, Watson MB, O'Kane SL, Drew PJ, Lind MJ, Cawkwell L. Mol Cancer Ther. 2006; 5:2115. [PubMed: 16928833]
69. Clausell-Tormos J, Lieber D, Baret JC, El-Harrak A, Miller OJ, Frenz L, Blouwolff J, Humphry KJ, Köster S, Duan H, Holtze C, Weitz DA, Griffiths AD, Merten CA. Chem Biol. 2008; 15:427. [PubMed: 18482695]

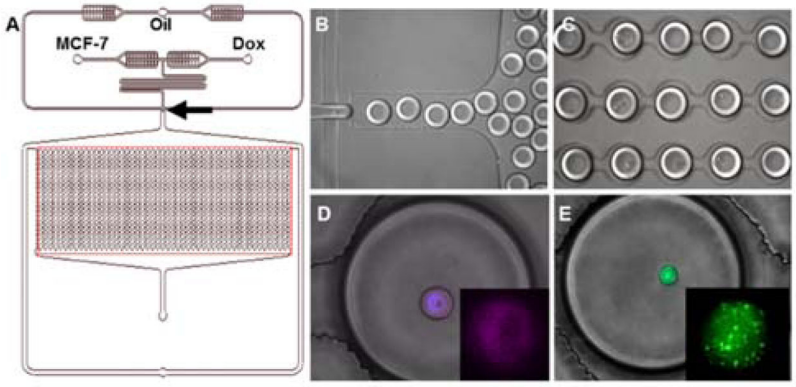

Fig. 1.

Single cell encapsulation in microfluidic droplet array. (A) Schematics of integrated microfluidic platform. The arrow indicates the droplet generation junction, and the boxed region indicates the droplet docking array. (B) Droplet generation. (C) Droplet docking in microarray. (D) Detection of Cy-5 conjugated ABCB-1 mRNA in live MCF-7S cell in droplet (enlarged in Inset). The nucleus was labeled with Hoechst. (E) Dox-resistant MCF-7R cell encapsulation in droplet. Inset: Calcein AM localization in vesicles.

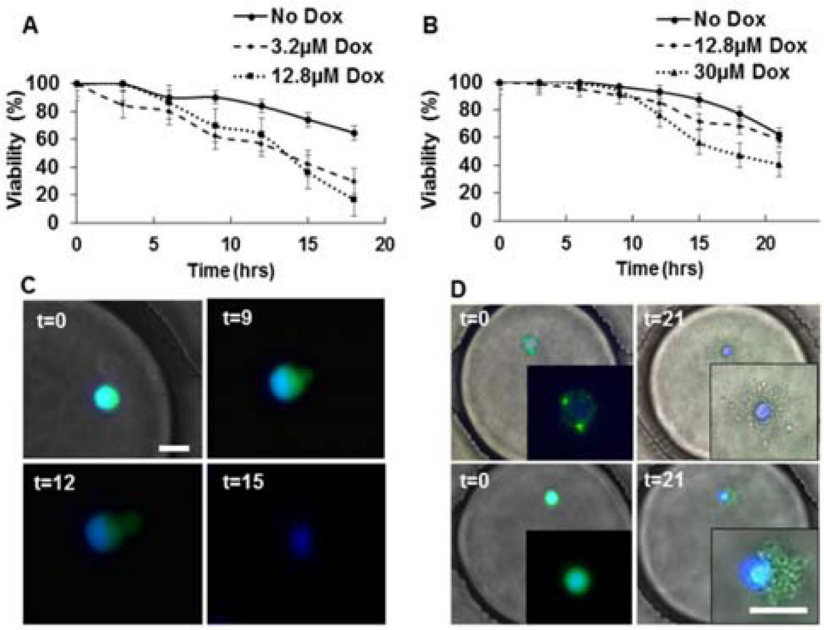

Fig. 2.

Dynamic Analysis of MCF-7 cell viability in droplets. (A) Cumulative viability (%) of MCF7 Dox-sensitive (MCF-7S) cells treated with 12.8μM or 3.2μM Dox compared to control condition (No Dox). (B) Viability of MCF7 Dox-resistant (MCF-7R) cells treated with No Dox, 12.8μM or 30μM Dox. (C) Morphology of typical MCF-7S cell death in droplets over time (in hours). (D) Morphology of two MCF-7R cell deaths in droplets. All cells were labeled with Calcein AM (green) and Hoechst (blue). Insets show enlarged view of the cells. Scale bar: 20μm

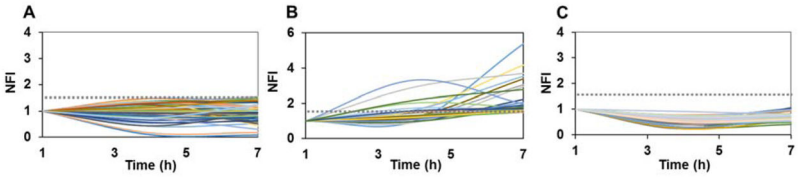

Fig. 3.

Trends in Dox uptake in MCF-7 cells. Single cells were treated with 12.8μM Dox in droplets. The dotted grey line is set at an arbitrary threshold 1.5. (A) MCF-7S cells showing relatively constant or slight decrease in intracellular fluorescence. (B) MCF-7S cells showing increase in Dox fluorescence over time. (C) Dox levels in MCF-7R cells. NFI: Normalized Mean Fluorescence Intensity, calculated as time-dependent fold change in background-corrected intensity values of same cells.

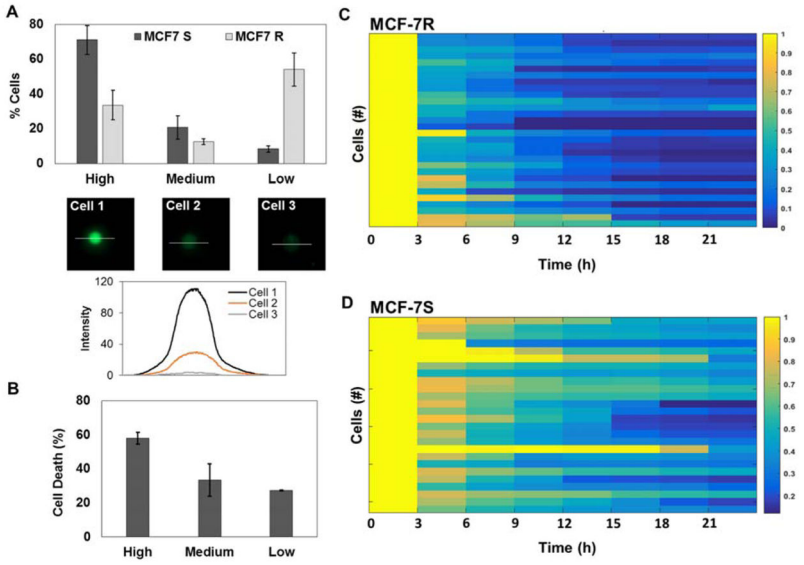

Fig. 4.

Quantification of Calcein AM uptake by MCF-7S and MCF-7R cells. (A) Comparison of cells exhibiting various levels of Calcein AM fluorescence in droplets. Representative images and intensity profile of cells depicting high (Cell 1), medium (Cell 2) and low (Cell 3) fluorescence are shown. The intensity profiles of the cells were calculated along the indicated white lines. (B) Total % of MCF-7R cell death in each category. MCF-7R cells were treated with 12.8μM of Dox in droplets. (C) Heat map of Calcein AM efflux profiles of MCF-7R cells from one experiment. (D) Representative heat map of Calcein AM efflux profiles of MCF-7S cells.

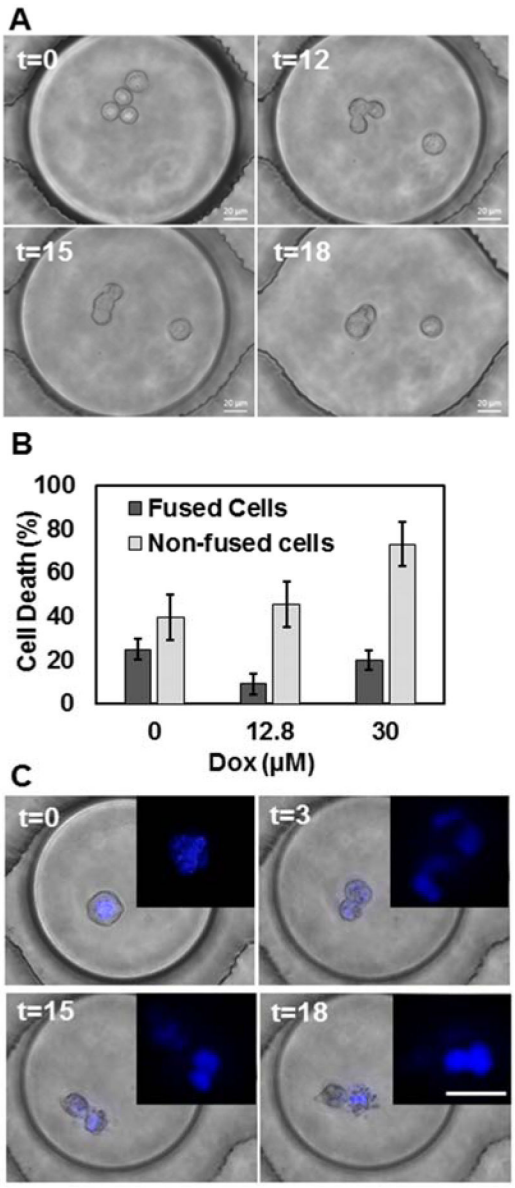

Fig. 5.

(A) Homotypic cell aggregation and fusion in droplets. (B) Quantitative analysis of MCF-7R cell death based on fusion. (C) Aberrant nuclear division and subsequent cytoplasmic deformation (nuclei enlarged in Inset). Scale bar: 20μm.